



HAL
open science

Real-time optical fibre near-infrared chromatic dispersion analyser using collocated optical fibre gratings

Thomas Allsop, Andreas Ioannou, Kyriacos Kalli, Ranjeet S. Bhamber, Evelyne Aguera, Alain Samson, Peggy Rigou, Cédric Saucier, Bernard Dussardier

► To cite this version:

Thomas Allsop, Andreas Ioannou, Kyriacos Kalli, Ranjeet S. Bhamber, Evelyne Aguera, et al.. Real-time optical fibre near-infrared chromatic dispersion analyser using collocated optical fibre gratings. *Optics Express*, 2024, 32 (23), pp.41026-41040. 10.1364/OE.530983. hal-04792863v2

HAL Id: hal-04792863

<https://hal.science/hal-04792863v2>

Submitted on 16 Dec 2024

HAL is a multi-disciplinary open access archive for the deposit and dissemination of scientific research documents, whether they are published or not. The documents may come from teaching and research institutions in France or abroad, or from public or private research centers.

L'archive ouverte pluridisciplinaire **HAL**, est destinée au dépôt et à la diffusion de documents scientifiques de niveau recherche, publiés ou non, émanant des établissements d'enseignement et de recherche français ou étrangers, des laboratoires publics ou privés.



Distributed under a Creative Commons Attribution 4.0 International License



Real-time optical fibre near-infrared chromatic dispersion analyser using collocated optical fibre gratings

THOMAS ALLSOP,^{1,2,8}  ANDREAS IOANNOU,³ KYRIACOS KALLI,³ 
RANJEET S. BHAMBER,⁴ EVELYNE AGUERA,⁵ ALAIN SAMSON,⁵
PEGGY RIGOU,⁶ CEDRIC SAUCIER,⁶
AND BERNARD DUSSARDIER^{7,9} 

¹Aston Institute of Photonic Technologies, Aston University, Aston Triangle, Birmingham, B47ET, UK

²Engineering and Technology, University Centre Grimsby, Grimsby, Lincolnshire, DN34 5BQ, UK

³Cyprus University of Technology, PhOSLab, Limassol, 3036, Cyprus

⁴Dept. of Population Health Sciences, Bristol Medical School, University of Bristol, UK

⁵INRAE, UE999 Pech Rouge, Gruissan, France

⁶SPO, Université de Montpellier, INRAE, Institut Agro, 34000 Montpellier, France

⁷Université Côte d'Azur, CNRS, Institut de Physique de Nice (INPHYNI), Nice, France

⁸t.d.p.allsop@aston.ac.uk

⁹bernard.dussardier@univ-cotedazur.fr

Abstract: We present what we believe to be a novel optical fibre device for real-time measurements of near-infrared chromatic dispersion of a liquid medium from 1100 nm to 1700 nm. This inline optical fibre chromatic dispersion analyser is based upon collocated fibre long-period gratings written adjacently in the core by femtosecond laser inscription yielding 8 attenuation bands associated with different cladding modes, yielding 8 independent measurements. This fibre device is tested on a series of chemical compounds associated with wines. The results for each compound yielded distinctive chromatic responses. A machine learning pipeline was developed that successfully clustered and classified spectral responses of the different chemicals to illustrate the distinctive responses. The limits of detection for these fibre devices ranged from 1×10^{-3} to 6×10^{-5} mol/L for the compounds associated with wines, demonstrating the potential usefulness of an optical fibre chromatic dispersion analyser is capable of monitoring in real-time effective chromatic dispersion that is not offered by any current technology.

Published by Optica Publishing Group under the terms of the [Creative Commons Attribution 4.0 License](https://creativecommons.org/licenses/by/4.0/). Further distribution of this work must maintain attribution to the author(s) and the published article's title, journal citation, and DOI.

1. Introduction

Fibre long period gratings (LPGs) have been routinely used to measure the changes in refractive index of countless liquids by monitoring the wavelength shift and amplitude changes in one of the transmission spectrum attenuation bands. This has been realized using a number of configurations over the last couple of decades, from simple uniform LPGs to LPGs coated to yield index changes with chemical specificity [1,2].

LPG refractive index modifications typically have periods ranging from 100 to 500 μm and behave as a dispersive optical element, resulting in deep notches in the wavelength-based transmission spectrum of an optical fibre that contains the said LPG [3]. LPGs are therefore an attractive form of optical fibre sensor, due to an inherent sensitivity to strain, temperature, refractive index, bending and load/compression [4–6]. The transmission spectrum of the fibre LPG is characterised by several attenuation bands, with the centre wavelength λ_c of an attenuation

band specified by the phase-matching condition:

$$\delta n_{eff_v} \Lambda = \lambda_v \quad (1)$$

where $\delta n_{eff_v} = [n_{co}^{01}(\lambda, \varepsilon, T, R, n_1, n_2) - n_{cl}^{1v}(\lambda, \varepsilon, T, R, n_1, n_2, n_s)]$, where n_{co}^{01} is the effective index of the core mode, n_{cl}^{1v} the effective index of the v^{th} radial cladding mode, with both indices identifying the cladding mode order and a dependence on the refractive index and the optical fibre geometry, n_1 is the refractive index of the core, and n_2 the refractive index of the cladding and the wavelength λ . Moreover, n_{cl}^{1v} is a function of the refractive index of the surrounding medium, n_s . Λ is the LPG period, T the temperature and ε the strain (compression in this situation) experienced by the fibre along with R the curvature [3]. The quantity δn_{eff_v} is defined as the differential effective index between the core and cladding modes. The superscripts with respect to the core mode denote the $HE_{1,1}$ mode and in the case of the cladding modes refers to the $HE_{1,v}$ axially symmetric cladding modes. This assumes that the grating consists of a circularly symmetric index perturbation transverse to the fibre axis, so that the only non-zero coupling coefficients between the core mode and the cladding modes involve cladding modes of azimuthal order 1 [7].

There are other configurations of fibre LPG devices that utilize the material and waveguide dispersive properties of the optical fibre to produce dual-peak attenuation band resonance. This occurs where the phase-matching of the cladding mode to the core mode is at a dispersion turning point of the optical fibre [8]. These strategies have been employed to measure the refractive index of the surrounding medium at one or over a very small wavelength range, in fact over a few nanometers. However, LPGs usually have several attenuations over a very much larger spectral range, therefore the LPG can be used to estimate the chromatic dispersion relationship of the medium into which they are submerged. Refractive index measurements are usually obtained using a refractometer and in-line process refractometers are available commercially. However, these typically operate only at a specific wavelength [9], and do not produce a chromatic dispersion relationship. To measure chromatic dispersion, a rainbow or Wedge-cell technique is used [10,11] or an alternative approach to chromatic dispersion measurement is using liquid-prism surface plasmon resonance sensor [12]. However, these are based on free space optics, as is the more conventional method of ellipsometry [13]. In all cases, the analytical tests are performed by operatives within a controlled laboratory environment. A useful method to estimate chromatic dispersion would be to use the series of attenuation bands from a LPG structure to simultaneously measure the refractive index of a liquid at different wavelengths. The LPG would be designed to couple the core mode to different cladding modes associated with each attenuation band [14], to yield independent measurements, to arrive at the chromatic dispersion curve of the material in the near infrared spectral region. This would be the first time “full potential” implementation of the LPG fibre device concept is achieved by multiplexing several independent measurements at the same spatial location, simultaneously.

To achieve the aforementioned independent measurements, a fibre device was designed and fabricated based on two LPGs (“Bi-LPG”) written adjacent to each other (side by side) using a femtosecond laser inscription scheme in a standard single mode fibre (silica based, type G.652, numerical aperture of 0.14, core diameter 8.2 μm , germano-silicate core), with periods of 339 μm and 525 μm , respectively. This Bi-LPG yields 9 attenuation bands associated with 9 different cladding modes from 1100 nm to 1700 nm. Furthermore, to show the usefulness of this approach and to evaluate the Bi-LPG fibre device potential as an analytical tool, the fibre device was tested with a range of solutions containing chemical compounds that are present in many beverages at various concentrations. In discussion with the France National Research Institute for Agriculture, Food and Environment (INRAE), it became evident that wine and its associated chemicals would be a good example to demonstration of the Bi-LPG usefulness analytical tool. The monitoring of the wine process from must (i.e. unfermented pressed grapes) to final product is necessary

for better control of the process and the quality. Improving the efficiency of fermentations in addition to avoiding challenging situations like stuck fermentations or the production of hydrogen sulfide [15]. Conventional analytical techniques are employed already, such as, mid-infrared spectroscopy [16,17] but samples are taken to a laboratory environment to be tested, thus not an inline process and use traditional spectroscopy methods [17]. Creating an additional analytical tool for inline measurements would be of value to the wine manufacturing industry.

Therefore, a series of chemicals associated with wine production was investigated. By altering the concentration of the solution of these chemical components over the range found within commercial beverage, a measurable effect on the chromatic dispersion of those solutions was observed. Furthermore, these changes in the profile of the chromatic dispersion curves were unique for each chemical compound, hence offering an additional way to investigate and characterise the beverage as an entity. This is the first time that the “full near infrared” spectral behaviour of Bi-LPG has been exploited, that is, multiplexing several independent measurements (attenuation bands associated with different cladding modes) at the same spatial location over a large section of the near infrared spectrum (~1100 nm to 1700 nm). To separate the distinct spectral responses of the 8 attenuation bands, a machine learning pipeline was developed, which involved the spectral clustering of the signals using a uniform manifold approximation and projection for dimension reduction (UMAP), followed by cluster classification using a hierarchical clustering approach (HDBSCAN). The results showed independent spectral characteristics, combined with the machine learning pipeline that could classify the spectral response of the Bi-LPG for the chemicals used in the study.

In this paper, to the authors knowledge, the first purposely designed inline optical fibre chromatic dispersion analyser based upon collocated fibre long period grating (Bi-LPG) is presented. This is demonstrated by using 8 attenuation bands in the 1100–1700 nm wavelength range, associated with 8 different cladding modes in the transmission spectrum of the Bi-LPG. Thanks to the individual calibration of the attenuation bands wavelength shift to refractive index, their spectral responses to different chemical compounds at different concentrations in solution are studied. It is shown that the Bi-LPG sensor could distinguish the different chromatic dispersion relationships for each different chemical solution. Furthermore, using a machine learning pipeline in conjunction with the Bi-LPG spectral responses could be used to classify/identify chemicals. The paper is organised as follows. The section “Materials and methods” details the principle, the fabrication and the calibration of the Bi-LPG device, as well as the preparation of the tested compound solutions, the so called “model wines”. In the section “Experimental results” are reported the extracted dispersion curves obtained by testing the individual model wines over several orders of magnitude in terms of compounds concentration. In the “Discussion”, the dispersion results are analysed by developing a machine learning pipeline to successfully separate spectral features in the dataset. Also the limits of detection of each compounds by the presented Bi-LPG device are presented and discussed.

2. Materials and methods

2.1. Fibre device fabrication

The Bi-LPG were manufactured using femtosecond laser direct inscription in a standard optical fibre (type G.652, numerical aperture of 0.14, core diameter 8.2 μm) using a femtosecond laser Plane-by-Plane (PI-b-PI) technique, a highly customized inscription process through the coating, that provides precise control of the grating period, length, width, and depth of the grating planes [18,19]. Fibre samples were mounted on two-axis air-bearing translation stages (Aerotech), allowing for controlled movement during the inscription process. The femtosecond laser system generated 517 nm pulses of 220 fs duration, which were guided through a long working distance objective x50 (Mitutoyo) and focused inside the fibre using a third translation stage. The inscribed planes had a width of ~800 nm, while the other dimensions were adjusted by suitable translation

stage motion resulting in a 3-dimensional refractive index change with controlled plane length, depth, and grating-plane angle. The grating planes for each LPG were inscribed longitudinally inside the core and along the fibre core axis [20] and parallel with each other, separated by a 2 μm gap, with the same pulse energy of ~ 100 nJ and with a repetition rate of 5 kHz. To increase the number of channels within the transmission range 1100–1700 nm, two LPGs were inscribed side by side in the fibre. The first grating had a period of 525 μm and a total length of ~ 26.26 mm and the second one had a period of 339 μm and total length ~ 31.9 mm. Both gratings had a 50/50 duty cycle. After inscription, the LPGs have been annealed. The perceived asymmetric nature of this Bi-LPG that could lead to birefringence and coupling to higher order modes make the spectral response of the fibre device complicated and unrepeatable with regards to fabrication. This is not the case for several reasons. Firstly, the inscription is very close to the fibres central axis, with a 2 μm gap between each LPG, hence the structural asymmetry is negligible. Secondly, the secondary index modification of the femtosecond laser inscription is small because the Bi-LPG have been annealed, this dramatically reduces birefringence [21]. Thirdly, the model phase-matching predictions are based upon a radially symmetric step-index fibre. These predictions show reasonably good agreement with the fabricated Bi-LPGs transmission spectrum, i.e. the spectral location of the LPGs attenuation bands.

The Bi-LPG device was designed to obtain a maximum number of attenuation bands associated with different cladding modes, refer to Fig. 1(a). The periods were chosen by solving the analytical dispersion relationship for the propagation constant for the core and cladding mode with azimuthal dependence $\exp(\pm i l \phi)$, for an optical fibre [7]. A transmission spectrum of the Bi-LPG is shown in Fig. 1(b) for which the measurements were recorded at a temperature of 23.5 $^{\circ}\text{C}$ and in air. Figure 1(a) shows the predicted period versus wavelength phase matching curves for a standard telecommunication optical fibre (SMF 28/ type G.652), onto which are added the phase matching conditions for two LPGs having periods of 339 μm and 525 μm , respectively. The crossing points on the graph identify the anticipated spectral location of the LPG attenuation bands. Figure 1(b) shows the transmission spectrum of the fabricated Bi-LPG (periods 339 μm and 525 μm) and the associated $\text{HE}_{1,\nu}$ cladding modes of the attenuation band with a typical insertion loss of 2 dB.

This yields nine attenuation bands over a spectral range from 1100 nm to 1700 nm associated with different cladding modes, thus yielding nine well identified spectral transmission features for independent measurements of refractive index, from which a sampled measurement of chromatic dispersion is obtained. These are the dominant transmission spectral features from the Bi-LPG device. Furthermore, these spectral transmission features are the $\text{HE}_{1,\nu}$ cladding modes that have the greatest coupling coefficients between the core to the cladding modes. These $\text{HE}_{1,\nu}$ cladding modes have less E-field nulls in the core region of the optical fibre and hence have greater E-field overlap with the fundamental core mode [7]. Inspecting Fig. 1(b), there are other smaller attenuation bands that match up with the period and phase matching curves in Fig. 1(a). These other transmission spectral features, predominantly caused by the 525- μm period LPG, are small and are characterized by a poor signal to noise ratio, thus increasing errors associated with the measurements. Thus they were not chosen for this investigation. Furthermore, inspecting phase-matching curve Fig. 1(a), there is a possibility of duplication of some attenuation bands at longer wavelengths by the same cladding modes, this is to be avoided because independent measurements by each attenuation bands is required.

There is an observable difference between the theory and the measured spectral location of the attenuation bands. This is likely due to the index modulation caused by the femtosecond inscription and an effective change in the bulk index of the core of the optical fibre due to the two separate LPG inscriptions (see Fig. 2(a)). This can shift the attenuation bands [13].

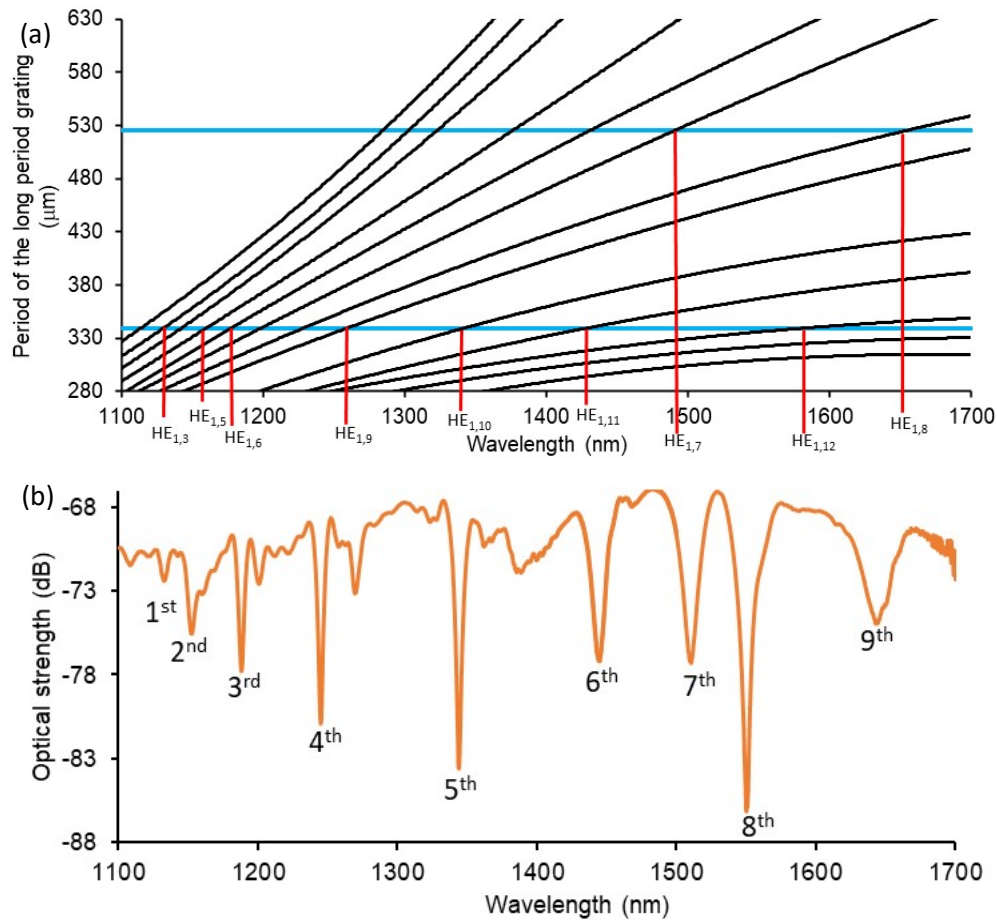


Fig. 1. (a) The predicted phase-matching curves for the attenuation bands for the cladding modes associated with a G.652 single mode telecommunication optical fibre. (b) The transmission spectrum of the fabricated Bi-LPG sensors with periods of 339 μm and 525 μm , for a 50% duty cycle in air and at a temperature of 23.5 $^{\circ}\text{C}$

2.2. Fibre sensor characterisation

The general procedure for determining the spectral index sensitivity of each attenuation band was performed by placing the Bi-LPG fibre sensor into a metallic V-groove machined into a flat aluminium plate, to minimise bending of the fibre. The V-groove was placed in contact with a granite optical table that acts as a heat sink and maintains a constant temperature. The optical fibre device/sensor was then successively immersed into calibrated index matching fluids that are at the same temperature as the V-groove. The calibrated index matching fluids are from Cargille laboratories. The calibrated refractive Index Liquids Series used are AAA full set of liquids 1.300-1.395 and part of AA series of 1.400-1.458 liquids. They have a quoted accuracy of ± 0.0002 . The Cauchy coefficients along with the index temperature coefficient for each liquid are provided by Cargille Labs.

The Bi-LPG fiber sensor was connected to a tungsten lamp (Ando AQ4305) to illuminate the sensor and to capture its transmission profile of each attenuation band for each index matching fluid. The LPGs transmission spectrum was collected by an optical spectrum analyser (Yokogawa, AQ6370D). The optical spectrum analyser has a resolution and accuracy of 0.05 nm. A schematic

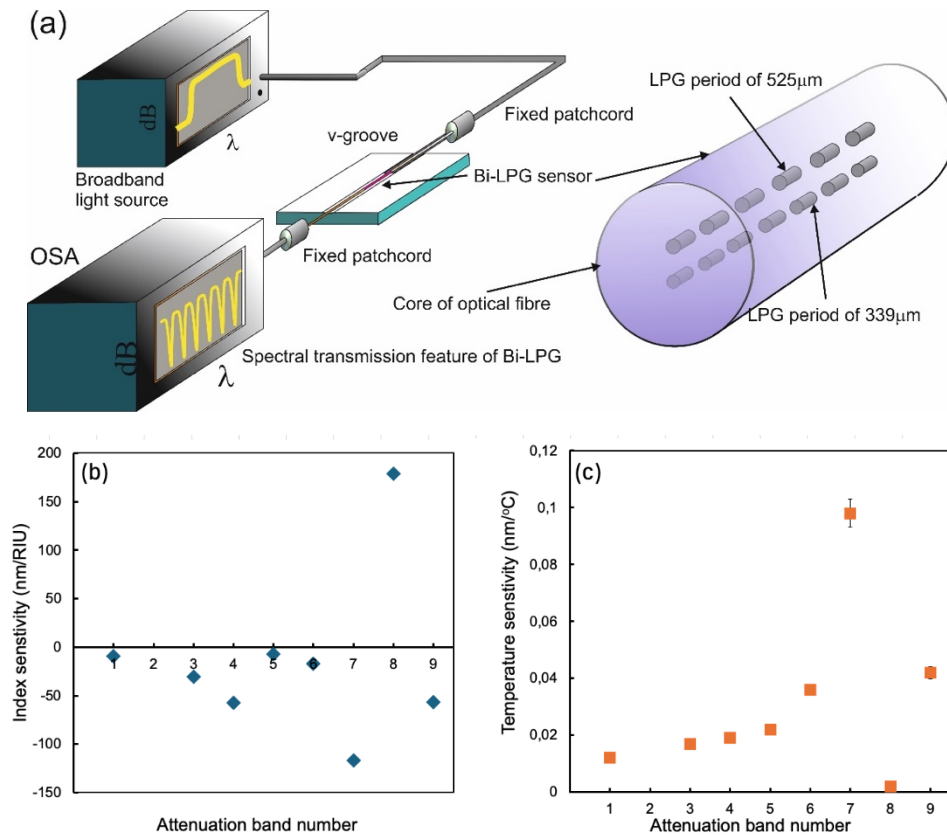


Fig. 2. (a) schematic of apparatus used for spectral wavelength sensitivities of the attenuation bands of the Bi-LPG fibre device with respect to (b) refractive index (c) temperature, errors are small compared to measurand.

of the apparatus is shown in Fig. 2(a). A 0.2-ml drop of a index fluid was set on the Bi-LPG, and the wavelength shift of each LPG band was recorded. Between two measurements, the Bi-LPG was rinsed in ethanol until all bands have recovered their initial spectral location, both in ethanol and in air. The temperature was measured at a precision of 0.1 °C to correct the transmitted spectra from slow temperature drifts from one day to the next. The central wavelengths of each band was calculated by using the first moment of the power spectrum, i.e. the centroid by geometric decomposition [14]. The centroid was evaluated with limits corresponding to the FWHM of the band, leading to approximately 120 data points. The minimal detectable wavelength shift is 6 pm, limited by the equipment. The associated error with this method was estimated with a stability measurement of transmission spectra of the Bi-LPG sensors taken over a 40-min interval. The error was estimated by calculating the standard deviation from the measured mean of 3 consecutive measurements of the combined wavelength and optical strength at the specific wavelength, divided by the root of the number of data points. This yields an error of ± 2 pm. Using this protocol, an empirical formula for refractive index sensitivity for each attenuation band has been obtained.

The characterisation of the sensitivity to temperature from 20 to 50°C was performed using the same apparatus and protocol, except that the sensor was placed on a peltier device. An empirical formula for wavelength shift (using the centroid method) as a function of temperature has been obtained.

The refractive index and temperature sensitivities are shown in Figs. 2(b) and 2(c), respectively. Following the calibration procedure, it was found that attenuation band 2 did not change monotonically with respect to temperature or index, hence this attenuation band was neglected for this demonstration. A possible reason for this spectral behaviour can be given by inspecting the phase matching curves of Fig. 1(a), for which there are several phase matching conditions for different cladding modes at this spectral location. We suspect that we observe a combination of attenuation features associated with different cladding modes, their net effect to yield a non-monotonic response to temperature and refractive index.

The central wavelengths were calculated by using the first moment of the power spectra; i.e. the centroid by geometric decomposition [22]. The centroid was evaluated with limits using the full width at half maximum (FWHM) leading to approximately 120 data points. The optical spectrum analyser has an accuracy of 0.05 nm. The associated error with this method was estimated with a stability measurement of transmission spectra of the Bi-LPG sensors taken over a 40mins time interval, with spectral noise having a standard deviation of $\Delta\lambda_{\text{error}} = 16$ pm and 2.2 m dB errors associated with the centroid measurement approach and measurement resolution of 6 pm. The attenuation bands spectral index sensitivity ranges from -117 to +179 nm/RIU with an average of 52 nm/RIU and the attenuation bands bandwidth ($\Delta\lambda_{\text{feature}}$) varies for each.

2.3. Analyte solution preparation

The base of all the synthetic solutions was a mixture of pure water, tartaric acid (33 mmol/L), ethanol (12%), and was adjusted at pH = 3.5 with NaOH. A set of chemical compounds were selected because they may be found in several beverages. The compounds included malic acid, lactic acid, acetic acid, ethyl-4 phenol acid, methional, sotolon, acetaldehyde, catechin and malvidin. A mother solution was sequentially diluted to span the concentrations on typical ranges 7.46 $\mu\text{mol/L}$ to 0.746 mol/L (e.g. malic acid) down to 30 nmol/L to 3 mmol/L (e.g. malvidin), for list of chemicals used and concentrations, see Table 1.

Table 1. Chemicals used in the investigation

Compound	Molar concentrations (mol/L)					
Catechin	3,45E-02	3,45E-03	3,45E-04	3,45E-05	3,45E-06	3,45E-07
Malic acid	7,46E-01	7,46E-02	7,46E-03	7,46E-04	7,46E-05	7,46E-06
Acetaldehyde	2,27E-02	2,27E-03	2,27E-04	2,27E-05	2,27E-06	2,27E-07
Lactic Acid	7,46E-01	7,46E-02	7,46E-03	7,46E-04	7,46E-05	7,46E-06
Sotolon	7,80E-03	7,80E-04	7,80E-05	7,80E-06	7,80E-07	7,80E-08
Methional	9,60E-03	9,60E-04	9,60E-05	9,60E-06	9,60E-07	9,60E-08
Ethly-4-phenol	2,46E-02	2,46E-03	2,46E-04	2,46E-05	2,46E-06	2,46E-07
Acetic Acid	3,33E-01	3,33E-02	3,33E-03	3,33E-04	3,33E-05	3,33E-06
Malvidin	3,02E-03	3,02E-04	3,02E-05	3,02E-06	3,02E-07	3,02E-08

3. Experimental results

3.1. Limit of detection

To test the potential of the Bi-LPG fibre device to do a sampled measurement of chromatic dispersion, we considered an interesting real-world application, that is the detection versus concentrations, in solution, of chemical compounds found in commercial drinks to determine the limit of detection (LOD). More importantly we aim to measure the chromatic material dispersion and determine if the Bi-LPG yields a distinctive spectral response to the chemicals. The analytes used are those typically found in wines. If successful, it would demonstrate potential as an

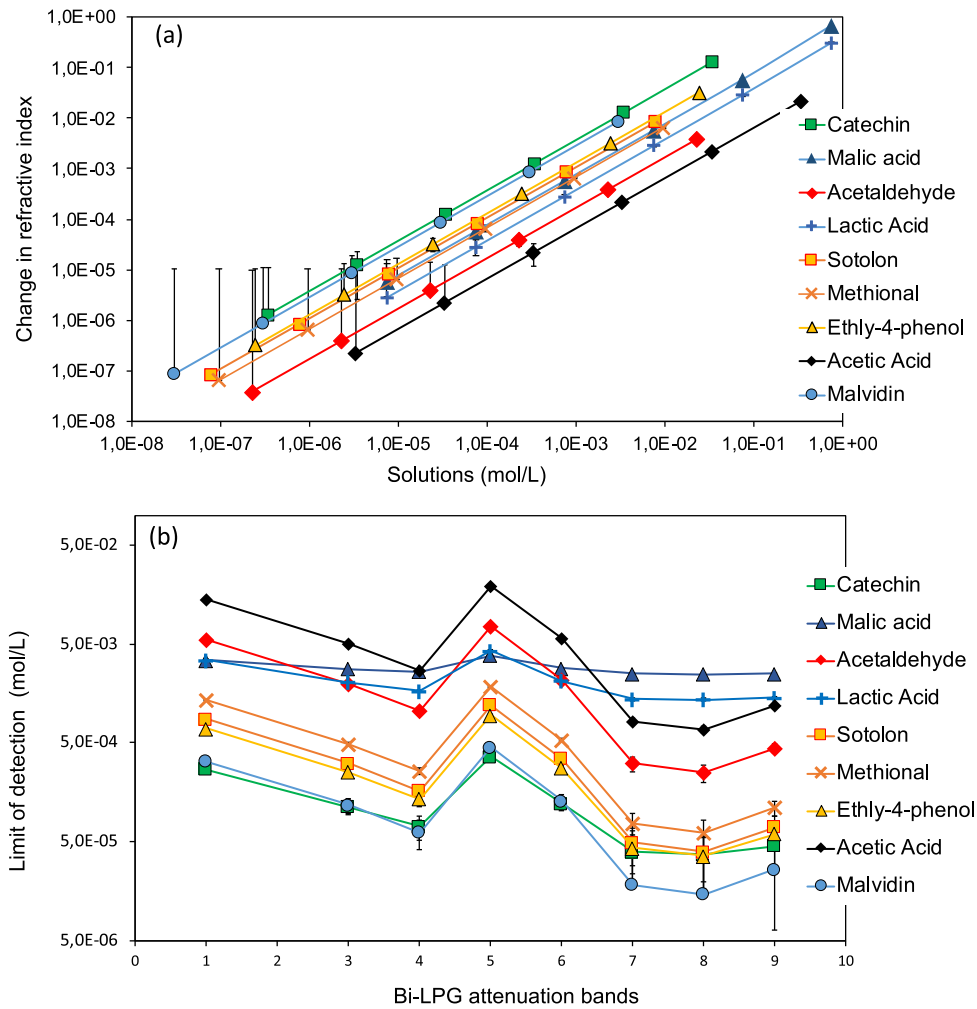


Fig. 3. (a). The estimated refractive index as a function of the chemical concentrations; (b) the estimated limit of detection of the attenuation bands of the Bi-LPG. All results have been temperature compensated to ensure the observed wavelength shifts are due to refractive index changes.

analytical tool for quality control in wine production, with reference to Table 1 and the method section.

The two important parameters that can be deduced from these results are the resolution, defined as $\Delta\lambda_{\text{error}}/(\text{refractive index sensitivity}; S\lambda_B)$, and the LOD. Note that LOD is dependent on the interrogation scheme, the light source spectral width, and the noise bandwidth of the measurement system. The LOD can be expressed in terms of standard deviation of noise of the sensor output $\Delta\lambda_{\text{error}}$, bulk sensitivity defined as $S\lambda_B = \Delta\lambda/\Delta n_s$ and bandwidth of the spectral transmission feature of the attenuation bands $\Delta\lambda_{\text{feature}}$. The FWHM of the resonance varied for each attenuation band and was used in determining the LOD. There are 120 discrete spectral data points per spectral scan across the resonant peak. The limit of detection is expressed as $\text{LOD} = \sqrt{((2 \cdot (\Delta\lambda_{\text{feature}} + \Delta\lambda_{\text{error}}))/120) S\lambda_B}$ [23]. Thus, the individual attenuation band will yield different index resolutions varying from 1.85×10^{-3} RIU to 8.34×10^{-5} RIU. The estimated LODs for the different attenuation bands associated with the various compounds, is shown in

Fig. 3. The index variation with differing concentrations was determined using the Maxwell Garnett Mixing Formula [24] and estimating the volume fraction by using the molar volume and a multiplying factor given by the concentration of the compounds within the solution and the spectral sensitivities of the attenuation bands, see Fig. 3(a). The estimated LOD for the compounds used are shown in Fig. 3(b) and are consistent with experimental results for the different chemicals, as shown later in the paper. Whilst the smallest changes in refractive index are shown in Fig. 3(a), in practical experiments, the temperature was monitored with an accuracy of 0.1°C . The smallest index changes would be dominated by the random variations in temperature of 0.05°C that would lead to 1.3 pm fluctuations, a value that is the equivalent of approximately 3×10^{-5} RIU.

3.2. Sensors experimental performances

The experiments procedure for index and temperature measurements on the model wines uses the same apparatus and protocols detailed in section 2.1. The Bi-LPG sensor is immersed into one of the model wine solution, both temperature is recorded and wavelength shift (using the centroid method) due to the chemical's refractive are measured. Corrections to compensate possible temperature drifts are performed using the empirical formula obtained during the calibration stage. This is done for each attenuation band at the 8 different spectral locations. Before each measurement is taken, the Bi-LPG is cleaned by washing with ethanol until all bands had recovered their their initial spectral location, both in ethanol and in air. Therefore, this yields measurements of refractive index of the chemical at different wavelengths over aforementioned wavelength range, thus yielding an estimate of the chromatic dispersion of the chemical.

Two examples of the wavelength shift for four attenuation bands are shown for malvidin and two of the sotolon solutions, see Fig. 4. These results are consistent with spectral characterisation of the attenuation bands with respect to their index spectral sensitivity and LOD of refractive index change. The LOD for the Malvidin is 1.8×10^{-5} mol/L and 1.4×10^{-5} mol/L solutions for 7th and 8th attenuation band, respectively, of the Bi-LPG (Fig. 3(b)). Lowering the molar concentration below these LOD leads to a plateauing of the wavelength spectral response (Fig. 4(a)). The wavelength shifts of the attenuation bands with smaller index spectral sensitivity, like bands 3 and 4, yield lower performance, typically a concentration LOD in Malvidin of $\sim 10^{-4}$ mol/L (Fig. 4(b)). A similar spectral response is also seen for the sotolon solutions with a concentration less than $\sim 5 \times 10^{-5}$ mol/L, see Fig. 4(c) detection of lower concentrations.

The various chemical species at different concentrations produced dissimilar spectral behaviour across the eight attenuation bands. Four examples of different chemicals are shown in Fig. 5. Firstly, the concentrations of the various chemicals are those found in usual beverages, such as wine. Inspecting the four examples, though the wavelength shifts are small (a few 10s of pm), there are distinct differences in the spectral responses for each solution. This would suggest that the Bi-LPG fibre device has spectral functionality to potentially identify different chemicals within a given solution via the refractive index measurement. Two examples are shown in Fig. 6, where the chromatic dispersion relationship of the solution as a function of concentration yields distinctive wavelength changes with refractive index. The lines connecting the points are polynomial interpolation (splines) of the measured points. The refractive indices are obtained by the experimental procedure described above.

The data shown in Fig. 6 are typical results obtained from the other chemicals used in this investigation with this type of fibre optical device. Inspecting Fig. 6(a) and 6(c), they have similar refractive index as a function of wavelength for lowest concentration, the refractive index yields a “W-curve” in the chromatic dispersion curve of the buffer solution (tartaric acid, ethanol, see section 2.3 above) which is the same for all analytes and contains the dominant chemicals at the lowest concentrations.

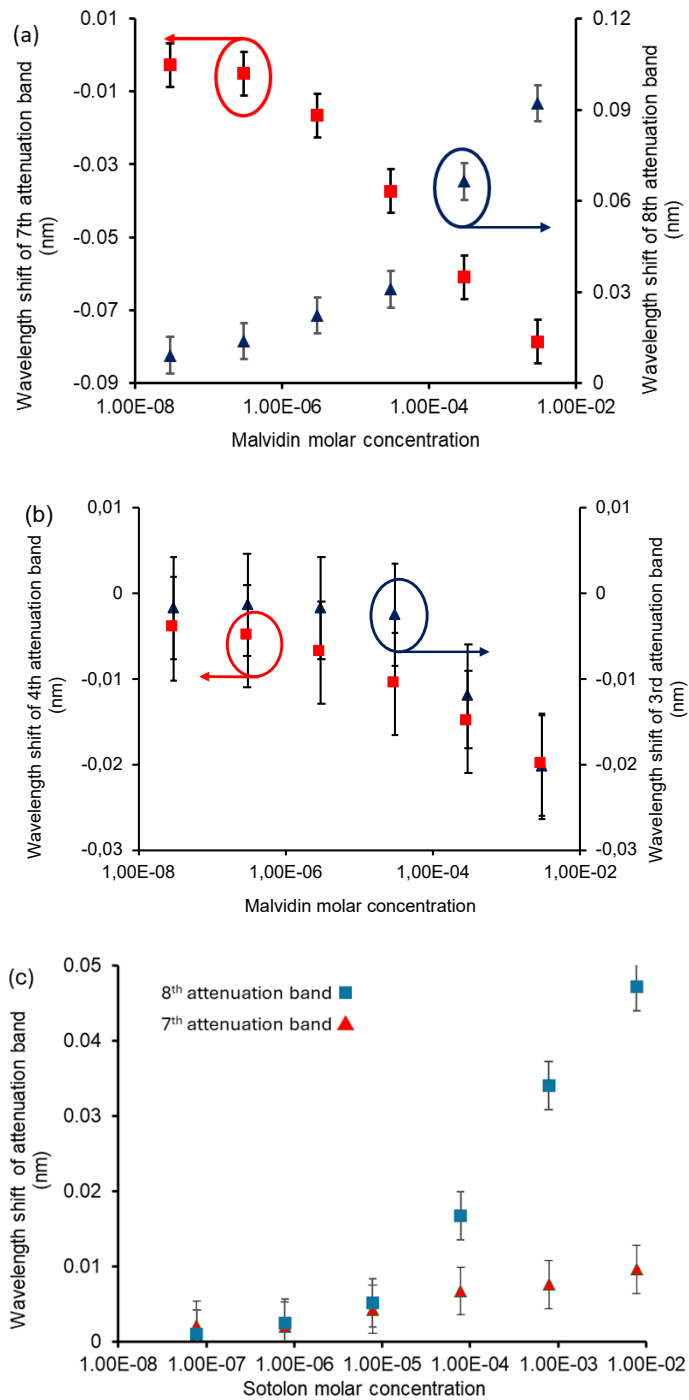


Fig. 4. Examples of the spectral response of particular attenuation bands of the Bi-LPG as a function of concentration (temperature corrected). (a) The wavelength shifts of the 7th and 8th attenuation bands (b) and the wavelength shifts of the 3rd and 4th attenuation bands for various concentrations of the Malvidin solution. (c) The wavelength shifts of the 7th and 8th attenuation bands for various concentrations of the sotolon solution.

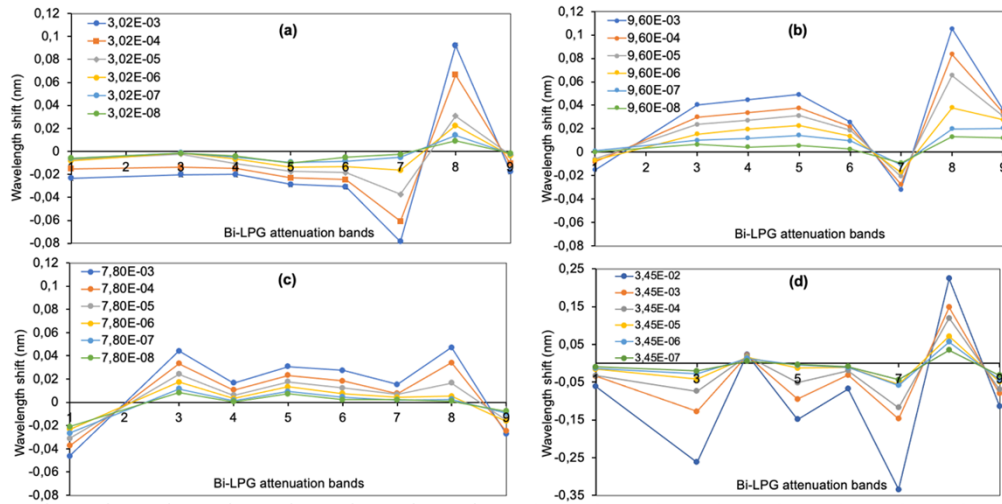


Fig. 5. Wavelength shift of the Bi-LPG attenuation bands at various molar concentrations of chemicals (expressed in mol/L), (a) malvidin, (b) methional, (c) sotolon and (d) catechin, error bars are ($\pm 1.3\text{pm}$), size of the markers.

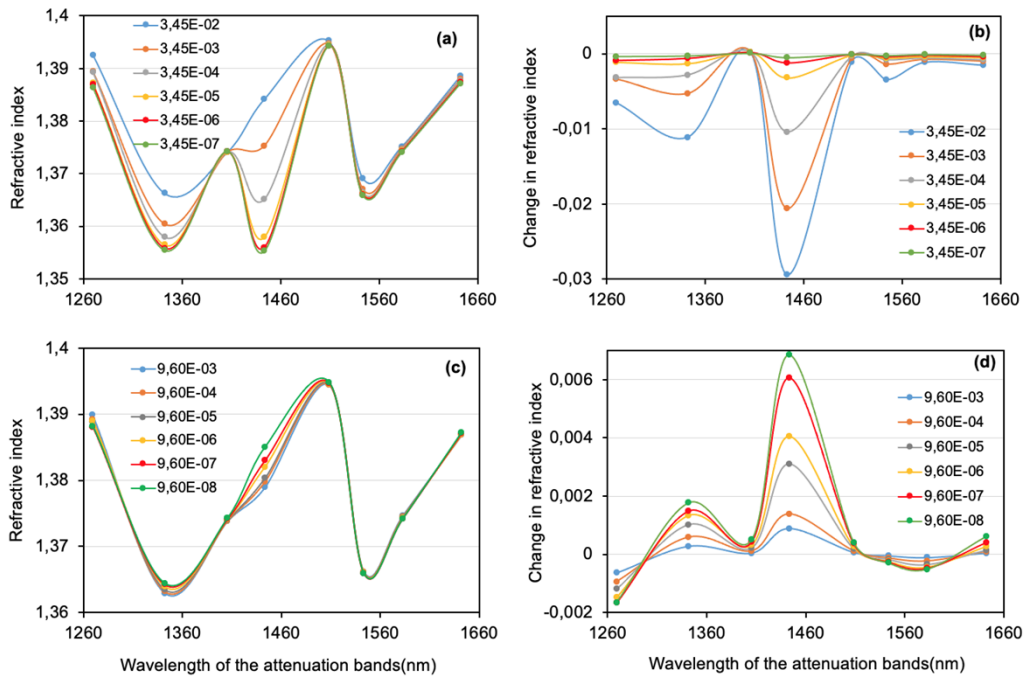


Fig. 6. The measured variation of chromatic dispersion as a function of molar concentration (mol/L) (a and b) of catechin solutions, and (c and d) methional solutions, the connecting lines are polynomial interpolation (splines) of the measured points. Wavelength error are ($\pm 1.3\text{pm}$) and refractive index errors 3×10^{-5} RIU is size of the markers.

The wavelength shifts are only investigated here because the optical strength of the attenuation bands remained reasonably constant throughout the experiments, which is expected due to the small changes in the refractive index and the lesser optical strength spectral sensitivity. The largest

index change observed is for Malvidin with an index change Δn ranging from $\sim 3.3 \times 10^{-2}$ to $\sim 3.3 \times 10^{-5}$, whereas the majority of the compounds show a typical index change of approximately 3.3×10^{-4} and negligible changes in the optical strength.

4. Discussion

The flexibility associated with the femtosecond laser inscription allows fabrication of Bi-LPGs with periods that generate the attenuation bands located in the spectral range 1100 nm to 1690 nm,

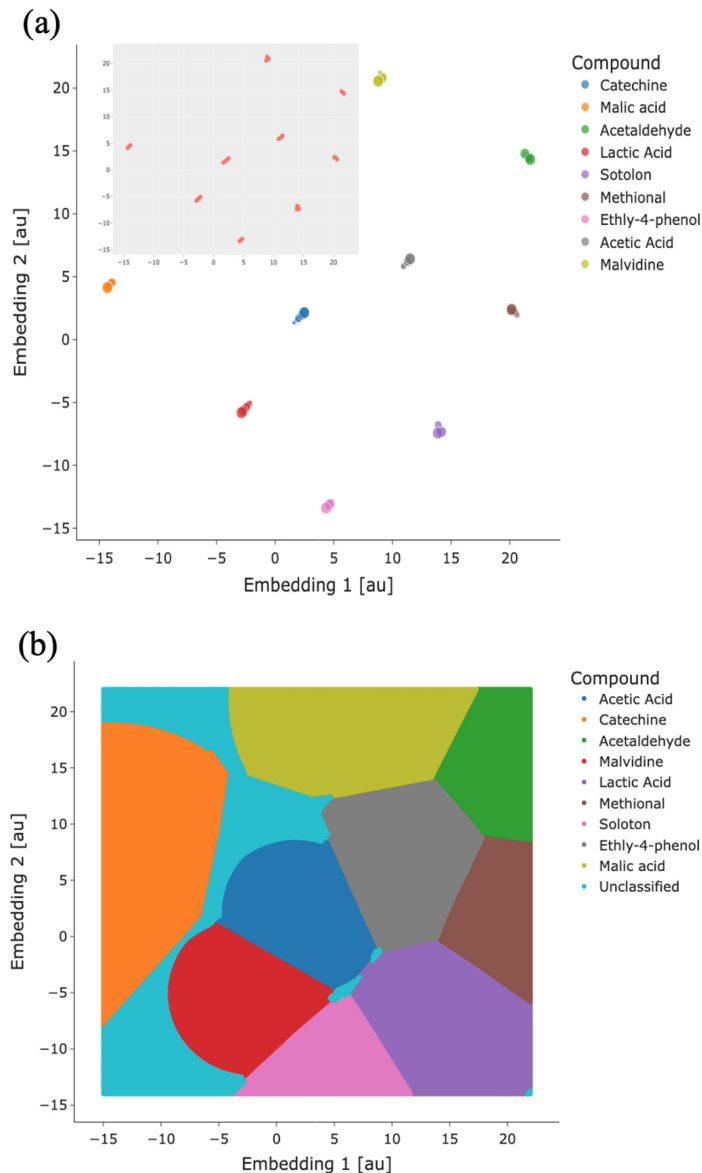


Fig. 7. The Dimensional reduction and information compression of wavelength shift of the various chemicals. (a) Machine learning pipeline results using UMAP for dimensionality reduction and clustering and HDBSCAN cluster classification. (b) The classification map of the chemical producing from the clustering result.

with first attenuation band at 1134.4 nm and 9th attenuation band at 1644 nm. Each transmission feature is associated with a different cladding mode ($HE_{1,\nu}$), yielding independent refractive index measurements at the same spatial location, producing a sampled measurement of the fibre's chromatic dispersion and any associated change with its surroundings. Figures 5 and 6 show examples of the wavelength shift response for the chemicals investigated at various concentrations. They show that “collective wavelength” changes are distinctive from each other and this was also found in the variation of chromatic dispersion relationship for each chemical.

The distinctiveness of the chemicals spectral behaviour was investigated firstly using Principal Component Analysis [25] for dimensionality reduction and information compression to observe the independence of the Bi-LPG spectral response for all chemicals. The Principal Component Analysis approach was only partially successful at higher concentrations with overlapping at the lower concentrations. A machine learning pipeline was developed to correctly separate spectral features in the embedding space of the dataset and classify spectral responses. The embedding stage consists of clustering the spectral response (in this case a dimensionality reduction of the dataset onto a 2D manifold). Here we utilized Uniform Manifold Approximation and Projection (UMAP) [26], which is a topological approach based on manifold learning techniques, where it constructs a high-dimensional graph representation of the data and optimizes a low-dimensional graph to be as structurally similar as possible to the high-dimensional graph. The successful application of UMAP technique yielded distinctive clusters of the various chemicals including those that are of low concentrations, see Fig. 7(a) insert. The classification of individual clusters consists of a Hierarchical Density-based Spatial Clustering of Applications with Noise (HDBSCAN) approach. HDBSCAN [27] is a hierarchical density-based clustering algorithm that characterizes clusters as areas of high density separated from other clusters by areas of low density. The algorithm is capable of identifying clusters of varying densities and shapes, making it a powerful tool for clustering complex datasets. The successful application of cluster identification and classification is shown in Fig. 7(a). The individual chemicals are grouped together and separated from each other, thus yielding a strong indicator that the individual spectral results are distinctive. Secondly, the increasing size of the marker indicates increasing concentrations, see Fig. 7(a).

The classification map of the embedding space is depicted in Fig. 7(b) and shows the classification regions associated with specific chemicals. When applying this machine learning pipeline with new spectral measurements, the measurements are mapped onto the embedding space in the appropriate classification area of the chemical. The turquoise region in the embedding space indicates regions where the spectral features cannot be correctly classified, this area is

Table 2. Estimation of the limit of detection for each chemical and each Bi-LPG attenuation band

Attenuation band	Catechin	Malic acid	Acetaldehyde	Lactic Acid	Sotolon	Methional	Ethly-4-phenol	Acetic Acid	Malvidin
	mol/L								
1	2,69E-04	3,44E-03	5,49E-03	3,45E-03	8,67E-04	1,36E-03	6,92E-04	1,41E-02	3,26E-04
3	1,13E-04	2,80E-03	1,96E-03	2,04E-03	3,10E-04	4,84E-04	2,50E-04	5,07E-03	1,16E-04
4	7,17E-05	2,63E-03	1,04E-03	1,67E-03	1,64E-04	2,56E-04	1,35E-04	2,70E-03	6,16E-05
5	3,61E-04	3,83E-03	7,57E-03	4,28E-03	1,20E-03	1,87E-03	9,53E-04	1,95E-02	4,49E-04
6	1,22E-04	2,83E-03	2,17E-03	2,12E-03	3,43E-04	5,36E-04	2,77E-04	5,61E-03	1,29E-04
7	3,94E-05	2,49E-03	3,08E-04	1,38E-03	4,90E-05	7,63E-05	4,33E-05	8,32E-04	1,84E-05
8	3,67E-05	2,48E-03	2,47E-04	1,36E-03	3,94E-05	6,13E-05	3,57E-05	6,76E-04	1,48E-05
9	4,54E-05	2,52E-03	4,43E-04	1,44E-03	7,02E-05	1,09E-04	6,02E-05	1,18E-03	2,64E-05

minimal when compared to the rest of the map, and important in detecting errors in the spectral measurement.

The LOD are estimated by using polynomial regression to data points that have gradients with adjacent data with different concentrations and using the Δ error at the limit to distinguish individual measurements. Considering the application of Bi-LPG to investigate model wines, it was found that the LOD of the majority of the compounds is below the usual concentrations found in usual beverages, such as wine. The LOD values are shown in Table 2. These results show the potential of such a chromatic dispersion LPG fibre device.

5. Conclusion

It is not possible to compare such an in-situ device with other sensors because the in-line/in-situ devices only measure at a single wavelength, thus measuring a single refractive index and not chromatic dispersion curve of the surrounding medium. Moreover, we have shown that their individual specific chromatic dispersion curves for a given solution have the potential to produce distinctive responses using the above machine learning algorithm that can be used to identify various chemical components within a solution. This illustrates the usefulness of the Bi-LPG fibre device as a new analytical tool for monitoring in real-time in-line processes. Furthermore, this is the first time that the “full near infrared” spectral behaviour of a fibre LPG device has been exploited, that is, multiplexing several independent measurements (attenuation bands associated with different cladding modes) at the same spatial location at the same time which is utilizing the full sensing potential of the LPG sensing device and new sensing paradigm for LPGs.

Funding. University of Hull; Engineering and Physical Sciences Research Council (EP/R004900/1); Centre National de la Recherche Scientifique (Work contract # 1027296); Institut National de Recherche pour l’Agriculture, l’Alimentation et l’Environnement.

Acknowledgments. Author contributions are as follows: T. A. developed the original concept. T.A., B.D. modelled, designed and performed experiments, A. I., K. K. fabricated the Bi-LPG fibre devices. E.A. P.R. C.S. produced the various solutions used in the experiments. R.B. performed the machine learning and statistical analysis on experimental data. T. A., B.D. developed explanation for sensor behaviour. The manuscript was written by T.A., B. D., A. I., K.K., R. B., E.A., P. R., and C. S. All authors discussed the results and commented on the manuscript

Disclosures. The authors declare no conflicts of interest.

Data availability. Data underlying the results presented in this paper are not publicly available at this time but may be obtained from the authors upon reasonable request.

References

1. T. Allsop, L. Zhang, and I. Bennion, “Detection of organic aromatic compounds in paraffin by a long-period fibre grating optical sensor with optimized sensitivity,” *Opt. Comms.* **191**(3-6), 181–190 (2001).
2. W. Gan, Z. Xu, Y. Li, *et al.*, “Rapid and sensitive detection of *Staphylococcus aureus* by using a long-period fiber grating immunosensor coated with egg yolk antibody,” *Biosens. and Bioelectron.* **199**, 113860 (2022).
3. T. Allsop, D. J. Webb, and I. Bennion, “A comparison of the sensing characteristics of long period gratings written in three different types of fiber,” *Opt. Fib. Technol.* **9**(4), 210–223 (2003).
4. A. Vengsarkar, P.J. Lemaire, J.B. Judkins, *et al.*, “Long-period gratings as band-rejection filters,” *J. Lightwave Technol.* **14**(1), 58–65 (1996).
5. V. Bhatia and A.M. Vengsarkar, “Optical fibre long-period grating sensors,” *Opt. Lett.* **21**(9), 692–694 (1996).
6. H.J. Patrick, A.D. Kersey, and F. Bucholtz, “Analysis of the response of long period fibre gratings to external index of refraction,” *J. Lightwave Technol.* **16**(9), 1606–1612 (1998).
7. T. Erdogan, “Cladding-mode resonances in short- and long-period fibre grating filters,” *J. Opt. Soc. Am. A* **14**(8), 1760–1773 (1997).
8. Q. Ling, Z. Gu, and K. Gao, “Smart design of a long-period fiber grating refractive index sensor based on dual-peak resonance near the phase-matching turning point,” *Appl. Opt.* **57**(10), 2693–2697 (2018).
9. J. U. Porep, D. R. Kammerer, and R. Carle, “On-line application of near infrared (NIR) spectroscopy in food production,” *Trends Food Sci. Technol.* **46**(2), 211–230 (2015).
10. D. Luo, J. Xie, P. Zhang, *et al.*, “The measurement of chromatic dispersion of liquids based on rainbow technology with empirical mode decomposition,” *Laser Phys.* **31**(7), 075602 (2021).
11. K. A. Rutkowska, K. Orzechowski, and M. Sierakowski, “Wedge-cell technique as a simple and effective method for chromatic dispersion determination of liquid crystals,” *Photon. Lett. Poland* **8**(2), 51–53 (2016).

12. G. Lan, Y. Gao, and X. Zhang, "Measurement of chromatic dispersion of liquid in a wide spectral range based on liquid-prism surface plasmon resonance sensor," *Sens. and Bio-sens. Res.* **16**, 32–36 (2017).
13. M. Stchakovsky, Y. Battie, and A. En Naciri, "An original method to determine complex refractive index of liquids by spectroscopic ellipsometry and illustrated applications," *Appl. Surf. Sci.* **421**, 802–806 (2017).
14. D. Viveiros and M. M. M. José, "Spectral tuning of long period fiber gratings fabricated by femtosecond laser micromachining through thermal annealing," *MDPI Proc.* **15**, 4 (2019).
15. C. Gonzalez Viejo and S. Fuentes, "Digital assessment and classification of wine faults using a low-cost electronic nose, near-infrared spectroscopy and machine learning modelling," *Sensors* **22**(6), 2303 (2022).
16. C. Canal and B. Ozen, "Monitoring of Wine Process and Prediction of Its Parameters with Mid-Infrared Spectroscopy," *J. Food Process Eng.* **40**(1), e12280 (2017).
17. J. B. Johnson, K. B. Walsh, M. Naiker, *et al.*, "The use of infrared spectroscopy for the quantification of bioactive compounds in food: a review," *Molecules* **28**(7), 3215 (2023).
18. A. Ioannou, A. Theodosiou, C. Caucheteur, *et al.*, "Direct writing of plane-by-plane tilted fiber Bragg gratings using a femtosecond laser," *Opt. Lett.* **42**(24), 5198–5201 (2017).
19. A. Theodosiou, A. Lacraz, A. Stassis, *et al.*, "Plane-by-plane femtosecond laser inscription method for single-peak Bragg gratings in multimode CYTOP polymer optical fiber," *J. Lightwave Technol.* **35**(24), 5404–5410 (2017).
20. A. Theodosiou, R. Min, A. G. Leal-Junior, *et al.*, "Long period grating in a multimode cyclic transparent optical polymer fiber inscribed using a femtosecond laser," *Opt. Lett.* **44**(21), 5346–5349 (2019).
21. T. Allsop, M. Dubov, H. Dobb, *et al.*, "A comparison of the spectral properties of high temperature annealed long period gratings inscribed by fs laser, UV, and fusion-arc," In *Reliability of Optical Fiber Components, Devices, Systems, and Networks III*, SPIE, 176 Vol. 6193, (2006).
22. A.M. Bronstein, M.M. Bronstein, and R. Kimmel, *Numerical geometry of non-rigid shapes*. (Springer Science & Business Media, 2008).
23. R. D'Agata and G. Spoto, "Surface plasmon resonance imaging for nucleic acid detection," *Anal. Bioanal Chem.* **405**(2-3), 573–584 (2013).
24. V. Markel, "Introduction to the Maxwell Garnett approximation: tutorial," *J. Opt. Soc. Am. A* **33**(7), 1244–1256 (2016).
25. I. T. Jolliffe and J. Cadima, "Principal component analysis: a review and recent developments," *Phil. Trans. R. Soc. A.* **374**(2065), 20150202 (2016).
26. L. McInnes, J. Healy, and J. Melville, "UMAP: Uniform manifold approximation and projection for dimension reduction," *arxiv*, (2018).
27. C. Malzer and M. Baum, "A hybrid approach to hierarchical density-based cluster selection," in *2020 IEEE International Conference on Multisensor Fusion and Integration for Intelligent Systems (MFI)*, Karlsruhe, Germany, 223–228 (2020).